



저작자표시-비영리-변경금지 2.0 대한민국

이용자는 아래의 조건을 따르는 경우에 한하여 자유롭게

- 이 저작물을 복제, 배포, 전송, 전시, 공연 및 방송할 수 있습니다.

다음과 같은 조건을 따라야 합니다:



저작자표시. 귀하는 원저작자를 표시하여야 합니다.



비영리. 귀하는 이 저작물을 영리 목적으로 이용할 수 없습니다.



변경금지. 귀하는 이 저작물을 개작, 변형 또는 가공할 수 없습니다.

- 귀하는, 이 저작물의 재이용이나 배포의 경우, 이 저작물에 적용된 이용허락조건을 명확하게 나타내어야 합니다.
- 저작권자로부터 별도의 허가를 받으면 이러한 조건들은 적용되지 않습니다.

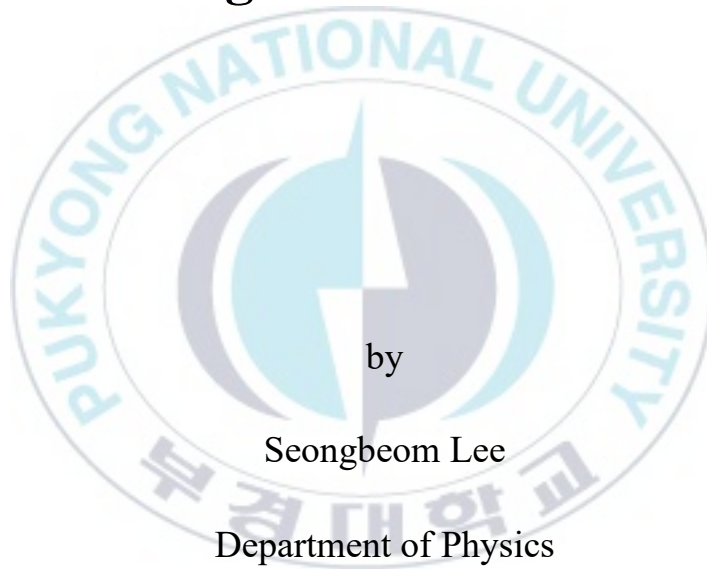
저작권법에 따른 이용자의 권리는 위의 내용에 의하여 영향을 받지 않습니다.

이것은 [이용허락규약\(Legal Code\)](#)을 이해하기 쉽게 요약한 것입니다.

[Disclaimer](#)

Thesis of Degree of Master of Natural Science

**High-performance Light Emitting Diodes  
based on Perovskite Nanocrystals via  
Surface passivation with Organic-  
Inorganic Additives**



by

Seongbeom Lee

Department of Physics

The Graduate School

Pukyong National University

August 2023

# High-performance Light Emitting Diodes based on Perovskite Nanocrystals via Surface passivation with Organic- Inorganic Additives

(유기-무기물 첨가제 도입을 통하여  
표면 결함이 제어된 고성능  
페로브스카이트 나노결정 발광 다이오드  
연구)

Advisor : Prof. Sung Heum Park

by  
Seongbeom Lee

A thesis submitted in partial fulfillment of the requirements  
for the degree of

Master of Natural Science  
in Department of Physics, The Graduate School,

Pukyong National University

August 2023

High-performance Light Emitting Diodes based on Perovskite  
Nanocrystals via Surface passivation with Organic-Inorganic  
Additives

A dissertation

by

Seongbeom Lee

Approved by

---

(Chairman) **Sung Heum Park**

---

(Member) **Bo Ram Lee**

---

(Member) **Hyosung Choi**

August 18, 2023

# Contents

List of Figures.....	ii
List of Tables .....	iv
Abstract.....	v
Chapter 1. Introduction .....	1
1.1 History of Perovskite Nanocrystals.....	1
1.2 Development of Perovskite LEDs.....	5
1.3 Working Principle of Perovskite LEDs.....	7
1.4 Characterization of Perovskite LEDs.....	9
1.4.1 Turn-on and Operating Voltage.....	9
1.4.2 Device Efficiency.....	10
Chapter 2. Research Background.....	11
Chapter 3. Experiment section.....	13
3.1 Materials .....	13
3.2 Preparation of DDAF precursor.....	14
3.3 Synthesis of CsPbBr <sub>3</sub> nanocrystals .....	14
3.4 Synthesis of Cadmium acetate treated CsPbBr <sub>3</sub> Nanocrystals.....	15
3.5 Device fabrication and characterization.....	16
Chapter 4. Result and Discussion .....	17
4.1 Concept of Surface passivation and TEM & PXRD analysis .....	17
4.2 Fourier-transform infrared spectroscopy and Optical analysis .....	21
4.3 Electrical analysis on PNCs and Perovskite LED.....	26
Chapter 5. Conclusion.....	33
Reference .....	34
Acknowledgement .....	38

## List of Figures

Figure 1. Structure of perovskite materials .....	2
Figure 2. Working principle of perovskite LEDs .....	8
Figure 3. Schematic band diagrams of perovskite LEDs.....	10
Figure 4. Schematic illustration of PNCs defect passivation and ligand exchange process .....	17
Figure 5. High magnification TEM image of pristine and CdAc treated CsPbBr <sub>3</sub> PNCs, size histogram of PNCs (inset).....	18
Figure 6. Low magnification TEM image of pristine and CdAc treated CsPbBr <sub>3</sub> PNCs and EDS mapping images of Cs, Pb, Cd and Br atoms .....	19
Figure 7. Powder X-ray diffraction pattern for pristine and CdAc treated PNCs.....	20
Figure 8. Fourier-transform infrared spectroscopy of neat, pristine and CdAc treated PNCs .....	21
Figure 9. Normalized absorption and PL spectra and UV-visible absorption of the pristine and CdAc treated PNCs .....	22
Figure 10. PL decay curves of the pristine and CdAc treated PNCs .....	23
Figure 11. Solution PLQY plots of the pristine and CdAc treated PNCs .....	24
Figure 12. Time dependent storage film PLQY plots of the pristine and CdAc treated PNCs .....	25

Figure 13. Photo of Time dependent storage film of the pristine and CdAc treated PNCs .....	25
Figure 14. $J$ - $V$ characteristics of hole-only devices with $V_{TFL}$ kink point behavior in pristine and CdAc treated PNCs films. ....	27
Figure 15. Energy level diagram of perovskite LED device.....	28
Figure 16. UPS spectra of pristine and CdAc treated PNCs .....	29
Figure 17. a) Current density–voltage ( $J$ – $V$ ) curves of perovskite LED device. b) Luminance–voltage ( $L$ – $V$ ) curves of perovskite LED device. c) Current density– EQE curves of perovskite LED device. d) EL spectra at $EQE_{max}$ of perovskite LED.....	29
Figure 18. EL spectra with voltage from 2.7 V to 4.5 V.....	30
Figure 19. Operational stability of pristine and CdAc treated perovskite LEDs measured at each current density .....	32
Figure 20. EL spectra at each point of operation.....	32
Figure 21. The temperature of both devices measured with an IR thermal imaging camera during the device’s operation.....	33

## List of Tables

Table 1. Summarized device performances with pristine and CdAc treated device..... 30



# High-performance Light Emitting Diodes based on Perovskite Nanocrystals via Surface passivation with Organic-Inorganic Additives

Seongbeom Lee

Department of Physics, The Graduate School,  
Pukyong National University

## Abstract

Halide perovskite nanocrystals (PNCs) demonstrate exceptional characteristics such as remarkable color purity, adjustability of emission wavelength, and a high photoluminescence quantum yield (PLQY). The efficiency and stability of perovskite light emitting diodes (LED) are influenced by the PLQY of the emitting layer and the density of traps. Thus, it is crucial to enhance the radiative recombination process through the reduction of surface defects in PNCs. In this thesis, I explored the utilization of cadmium acetate (CdAc) treatments with organic ligand engineering to passivate surface defects in PNCs. Our findings also indicate that the incorporation of cadmium ions can effectively reduce the formation energy of defects in PNCs via CdAc treatment. The results demonstrate that the implementation of CdAc treatment resulted in a decrease in the non-radiative recombination and defect density of PNCs. The optimized CdAc treated PNCs exhibited an enhanced PLQY of 96.02% in the green region (514 nm), as well as an efficient external quantum efficiency (EQE) of 20.79% when utilized in LED devices.

# Chapter 1. Introduction

## 1.1 History of Perovskite Nanocrystals

Perovskite compounds share a crystal structure akin to that of calcium titanate ( $\text{CaTiO}_3$ ), and are denoted by the general formula " $\text{ABX}_3$ ", where "A" represents a monovalent cation, such as methylammonium ( $\text{MA}^+$ ), formamidinium ( $\text{FA}^+$ ), or  $\text{Cs}^+$ ; "B" represents a divalent metal cation, such as  $\text{Pb}^{2+}$  and  $\text{Sn}^{2+}$ ; and "X" represents a halide anion, such as  $\text{I}^-$ ,  $\text{Br}^-$ , or  $\text{Cl}^-$ . The  $\text{ABX}_3$  perovskite crystal structure consists of monovalent "A" cations, which occupy eight apex angles, divalent "B" metal cations located at the body center, and halide "X" anions occupying six face centers. Figure 1 illustrates that "B" cations are coordinated with six "X" anions to form octahedra, which are interconnected by vertices to create a three-dimensional perovskite. The perovskite structure includes one "A" cation situated in the center of four octahedra. The stability of the cubic perovskite structure is evaluated using the octahedral factor  $\mu^{[1]}$  and Goldschmidt's tolerance factor  $t^{[2]}$ , which are calculated using the formulas which are shown Equation 1.1

$$t = \frac{r_A + r_X}{\sqrt{2}(r_B + r_X)}$$

Eq. 1.1

In this formula, the ionic radii of "A," "B," and "X" ions are represented by  $R_A$ ,  $R_B$ , and  $R_X$ , respectively. A stable cubic perovskite structure can be formed when the Goldschmidt tolerance factor  $t$  falls between 0.80 and 1.03 and the octahedral factor  $\mu$  exceeds 0.442.<sup>[3]</sup>

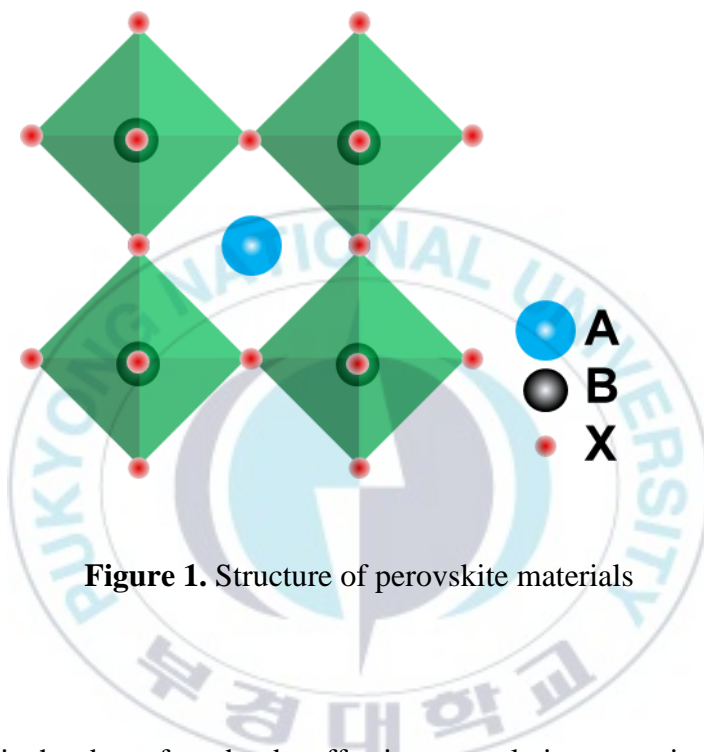


**Figure 1.** Structure of perovskite materials

Perovskite has been found to be effective not only in generating electricity by separating charges, but also in producing light by bringing charges together, despite this seeming counterintuitive.<sup>[4-6]</sup> They are attractive candidates for LEDs and lasers due to their low nonradiative recombination rates and high color purity.<sup>[7]</sup> However, the PLQY of bulk perovskite structures is limited due to two main factors: the presence of mobile ionic defects with low formation energy and a small exciton binding energy that leads to low electron-hole capture rates for radiative

recombination in metal halide perovskites.<sup>[8]</sup> In perovskite films made from precursor solutions, intrinsic defects were found to vary from grain to grain, with grain boundaries showing weak emission and faster nonradiative decay.<sup>[9]</sup> Therefore, researchers have shifted their focus to PNCs to improve PLQY and explore quantum confinement for tuning emission. In 2014, the first PNCs were created<sup>[10]</sup> and since then, research on these compounds has rapidly expanded. Organic capping ligands are used to control nanocrystals in the nanometer size range for PNCs, which can be shaped into PNCs or nanoplatelets, nanosheets, nanowires, and quantum dots. The size and shape of these PNCs can be finely tuned, even down to a single perovskite layer, leading to strong quantum confinement.<sup>[11-14]</sup> The composition, structure, and size of these PNCs can be adjusted not only during synthesis but also after synthesis, such as through ion exchange or exfoliation.<sup>[15-18]</sup> The band structure of PNCs allows for high photoluminescence (PL) efficiency, with defect states being either localized within the valence and conduction bands. PNCs are considered "defect-tolerant," as they require less passivation than metal chalcogenides. In recent years, PNCs have been optimized to emit throughout the visible spectral range with PLQY approaching 100%.<sup>[19-20]</sup> Using long chain ligand during the PNCs synthesis, the structural dimensionality of perovskite can be easily adjusted from 3D to 2D. The number of octahedral layers between the long-chain organic layers ( $n = 1$  to  $\infty$ ) determines the emission wavelength and exciton binding energies of the layered perovskites.<sup>[21-23]</sup> These

tunable properties, such as emission wavelength, narrow emission, and low nonradiative losses, make perovskite a promising candidate for LEDs. Moreover, perovskite possesses long charge carrier diffusion lengths that enable efficient recombination of electrically injected charge carriers. In contrast to bulk perovskites that suffer from low PLQY due to inherent defects, especially at grain boundaries, surfaces, and interfaces,<sup>[24-25]</sup> PNCs exhibit exceptionally high light-emitting efficiency with nearly 100% of PLQY. Despite having limited control over their size, shape, and colloidal stability, these reports showed that these fine PNCs had significantly increased emissivity. In late 2014, Gonzalez-Carrero *et al.*<sup>[26]</sup> reported an improved method for synthesizing highly luminescent MAPbBr<sub>3</sub> colloids in toluene. Although the particles had irregular shapes, as observed through transmission electron microscopy (TEM), they exhibited an impressive PLQY. The most notable colloidal synthesis for producing well-defined colloidal PNCs with controlled size distribution and thermodynamic stability was developed by Protesescu *et al.* in 2015.<sup>[27]</sup> This method, known as the hot-injection (HI) approach, was used to generate uniform CsPbX<sub>3</sub> NCs that had PLQY values of up to 100% and exhibited quantum-size effects like classical quantum dots (QDs). In 2015, Zhang *et al.* introduced the ligand-assisted reprecipitation (LARP) approach to synthesize MAPbX<sub>3</sub> PNCs with color-tunable emission and PLQY of up to 70% at room temperature (RT).<sup>[28]</sup> In general, treating PNCs with ligand molecules or metal halides after synthesis can significantly improve their PLQY, and functional

molecules can be used to achieve additional properties in PNCs.<sup>[29-31]</sup> The controlled synthesis of PNCs allows for easy testing of their potential applications in various devices, but their stability remains a major challenge. To address this issue, researchers have used *in situ* synthesis and post-synthetic surface coating strategies,<sup>[32-33]</sup> but these approaches often result in PNCs being coated with organic ligands, which can hinder the injection and transport of charge carriers. As a result, PNCs coated with dielectric shells are limited to use as down-converters in LEDs.

## 1.2 Development of Perovskite LEDs

In recent years, metal halide perovskite has shown remarkable properties suitable for next-generation optoelectronic devices such as LEDs,<sup>[34-36]</sup> solar cells,<sup>[37-38]</sup> and photodetectors<sup>[39]</sup> that are efficient and cost-effective. Perovskite LED offers advantages over conventional organic LEDs such as low-temperature fabrication, solution processing, and simple bandgap tunability. Compared to organic LEDs, perovskite LEDs generally provide better spectral purity and potential for high-brightness operation, making them desirable for large-area optoelectronic applications.<sup>[40]</sup> Recently, perovskite LEDs based on both 3D,<sup>[36, 41-43]</sup> QDs<sup>[44-45]</sup> and quasi-2D<sup>[46-47]</sup> perovskites have exceeded 20% EQE, which is a critical milestone for the development of perovskite LEDs. It has been shown that

near-100% PLQY<sup>[48]</sup> can be achieved through interfacial and compositional engineering,<sup>[49-50]</sup> solvent processing,<sup>[44]</sup> dimensionality control,<sup>[51]</sup> morphological optimization,<sup>[52]</sup> molecular passivation using polymers,<sup>[52]</sup> small-molecule additives,<sup>[42]</sup> and outcoupling enhancement.<sup>[46]</sup> The design philosophy for high-efficiency perovskite LEDs focuses on enhancing radiative recombination processes and suppressing non-radiative recombination processes in the perovskite emissive layers while eliminating undesirable carrier leakage and recombination through the charge-transport interfaces. The early designs of perovskite LED structures were inspired by device structures used in solution-processed organic LEDs and perovskite solar cells. In 2014, R. H. Friend *et al.* demonstrated the production of organic-inorganic hybrid perovskite LEDs at room temperature through solution spinning.<sup>[5]</sup> By adjusting the halogen composition and proportion, the emission range from near infrared to green was achieved, which initiated perovskite LEDs research. The following year, Tae-Woo Lee *et al.* produced a MAPbBr<sub>3</sub> perovskite device with a current efficiency of 42.9 cd/A.<sup>[53]</sup> They used the nanocrystal pinning spin coating process to reduce perovskite grain size, improve the film morphology, and minimize exciton quenching due to lead atoms. In 2018, Zhanhua Wei *et al.* reported a quasi-core/shell structure device with MABr shell passivated Cs-based perovskite, achieving an EQE of 20.3%<sup>[36]</sup> and a record for green perovskite LEDs. Currently, the EQE of green<sup>[54]</sup> perovskite LEDs have surpassed 28.9%.

### 1.3 Working Principle of Perovskite LEDs

Electroluminescence (EL) refers to the process where electrical energy is converted into light energy by a luminescent material under an applied electric field. In perovskite LEDs, when a voltage is applied to the electrodes, holes and electrons are injected from the anode and cathode, respectively. The injected charges then move towards the emissive layer, where they combine to form excitons, which are electron-hole pairs. Radiative transition of these excitons to the ground state results in light emission. The entire process can be divided into three steps: (1) Charge injection and transport, (2) Exciton formation, and (3) Exciton radiative transition.

Under the applied voltage, the anode injects holes to the highest occupied molecular orbital (HOMO) of the light-emitting layer, while electrons are injected into the lowest unoccupied molecular orbital (LUMO) of the emissive layer at the cathode. The injection barrier is due to the difference between the work function of the device electrode material and the HOMO/LUMO levels of the emissive layer. Therefore, the cathode is typically made of a metal with a low work function, while ITO with higher work function is used as the anode, which is often treated with ultraviolet (UV) ozone or plasma to improve its work function. The injected charges then move and drift in two directions under the applied electric field, and their mobility can be measured by space-charge limited current (SCLC).

Due to coulomb forces, electrons and holes recombine to form excitons, which typically form near the cathode and quench. To achieve balanced charge transport, suitable hole transport layer (HTL) and electron transport layer (ETL) can be introduced to control the migration of carriers. Excitons decay from the excited state to the ground state through radiative transitions, releasing photons and resulting in light emission. Theoretically, the generated excitons are singlet and triplet excitons in a ratio of 1:3. While fluorescent materials only release photons through singlet excitons radiation transition, phosphorescent material-based light-emitting devices can use all excitons during the light emission process. The theoretical internal quantum efficiency can reach 100%, which is four times that of fluorescent material-based LEDs.

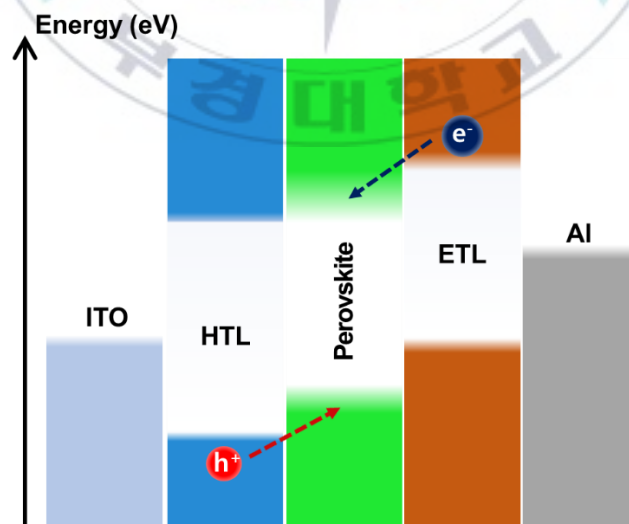


**Figure 2.** Working principle of perovskite LEDs

## 1.4 Characterization of Perovskite LEDs

The initial step towards achieving high-performance perovskite LEDs involves charge-transport layers with either hole-transporting (p-type) or electron-transporting (n-type) characteristics. These layers ensure balanced charge injection into the emissive perovskite layer and proper charge-blocking. One of the main challenges in selecting suitable HTLs and ETLs for perovskite emitters is finding charge-transport layers with compatible wide bandgaps that have the necessary energy levels and carrier mobilities to facilitate low-barrier and balanced charge transport. Additionally, these charge-transport layers should minimize non-radiative recombination losses at the interface, which is critical for achieving optimal device efficiencies.

### 1.4.1 Turn-on and Operating Voltage

Figure 3 shows that tunneling cannot occur under the zero-bias condition of the device due to the energy band's inclination. Upon applying a voltage equivalent to the disparity between the anode and cathode work functions, a "flat band" condition arises, and the turn-on voltage becomes the minimum threshold for injecting electrons and holes. The operating voltage, at which the current rapidly increases, indicates the successful tunneling of holes and electrons into the active layer.

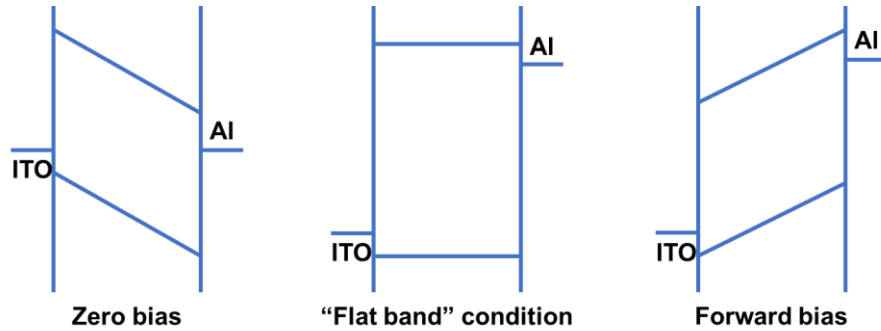


**Figure 3.** Schematic band diagrams of perovskite LEDs

### 1.4.2 Device Efficiency

The luminous efficiency of an LED is typically characterized using two metrics: current efficiency (CE) and EQE. CE is calculated as the luminous brightness per unit current density, measured in cd/A using the following formula:

$$\text{Current Efficiency (cd/A)} = \frac{\text{Luminance}}{\text{Current density}} * 10^{-1}$$

Equation.1.2

EQE of a device is determined by the ratio of the number of photons released externally from the device to the number of electrons injected into the external circuit, which is represented by the following formula:

$$\text{External Quantum Efficiency} = \frac{\text{The number of emitted photons}}{\text{The number of injected electrons}} * 100(\%)$$

Equation.1.3

## Chapter 2. Research Background

In recent years, advancements have been made in the development of LED technology using PNCs. This technology shows promise for next-generation RGB full-color display technology due to its remarkable optoelectrical properties, such as the ability to tune the emission wavelength by modifying the component and size of the PNCs, high color purity with narrow emission spectra, and high PLQY.<sup>[55]</sup> Research on LED technology has demonstrated that the PLQY of the emitting layer and the concentration of trap states are critical parameters that influence the efficacy and durability of the device. Thus, to augment the performance of perovskite LED, it is vital to regulate the surface defects of the PNCs to promote radiative recombination.<sup>[56]</sup> In general, PNCs that are produced synthetically are stabilized by the presence of long chain organic ligands such as oleic acid (OAc) and oleylamine (OLA). These ligands play a crucial role in the synthesis and stabilization of the PNCs' surface, leading to the formation of a uniform distribution. Nevertheless, PNCs that are capped with OLA and OAc tend to detach easily, resulting in poor colloidal stability and surface defects.<sup>[57]</sup> Although significant advancements have been made, concerns still exist surrounding the development of vacancies in the B-site cation of PNCs during the process of ligand exchange, which can result in non-radiative recombination.<sup>[58]</sup> Previous work demonstrated surface engineering techniques that can regulate the presence of B-site vacancies by incorporating different metal ions.<sup>[59]</sup> Meanwhile,

doping perovskite structures with metal ions can enhance the stability of the surface and decrease the density of defects. Specifically, previous investigations have indicated that it is possible to adorn the surface PNCs by introducing metal acetate additives onto their surface.<sup>[60]</sup> Consequently, it can lead to a rise in radiative recombination, improved stability, and the creation of highly luminescent and stable PNCs, thereby rendering them a suitable selection for perovskite LED applications. Hence, it is essential to suggest a potent approach that can curb the presence of surface defects in PNC via organic-inorganic surface engineering.

In this thesis, I explored the surface passivation of defects in PNCs via the use of CdAc and organic ligand engineering. Our findings suggest that the inclusion of CdAc treatments can elevate the radiative recombination rate of Cs-based green-emissive PNCs by hindering defects. The use of organic-inorganic engineered PNCs with CdAc and organic ligands produced a PLQY of 96.02% at 514 nm, compared to 67.18% for pristine PNCs. The surface treatment considerably lowered the density of defects and non-radiative recombination in PNCs. Upon being implemented in LED devices, the optimized CdAc-treated PNCs demonstrated a CE of 65.48 cd/A and an EQE of 20.79% in the green region.

## Chapter 3. Experiment section

### 3.1 Materials

Cesium carbonate (99.9%), Cadmium acetate dihydrate (reagent grade 98%), Cadmium acetate dihydrate (99.999% trace metals basis), 1-octadecene (ODE; 90% tech.), Oleylamine (OLA; 70% tech.), Oleic acid (OAc; 90% tech.), Methylacetate (MeOAc; anhydrous 99.5%), Octane (anhydrous  $\geq 99\%$ ), Toluene (anhydrous 99.8%), Hexane (anhydrous 95%), Chlorobenzene (anhydrous 99.8%), Lead bromide ( $\text{PbBr}_2$ ; 99.999% trace metal basis), poly[(9,9-dioctylfluorenyl-2,7-diyl)-co-(4,4'-(N-(4-sec-butylphenyl)diphenylamine))] (TFB) and Didodecyldimethylammonium bromide (DDAB; 98%) and sodium fluoride ( $\text{NaF}$ ; BioXtra,  $\geq 99\%$ ) were purchased from Sigma Aldrich. Poly[bis(4-phenyl)(2,4,6-trimethylphenyl)amine (PTAA; Mw : 30,000) was purchased from Ossila. Indium tin oxide-based transparent conductive electrode ( $\sim 4.5 \Omega/\text{sq}$ ) purchased from AMG.  $\text{MoO}_3$  (99.9995%) was purchased from Alfa Aesar. Aqueous solution of PEDOT:PSS (Clevios AI 4083) purchased from Heraeus. 2,2',2''-(1,3,5-benzinetriyl)tris(1-phenyl-1-H-benzimidazole) (TPBi; 99.9%) was purchased from OSM. LiF (99.9%), Ag (99.99%) and Al (99.9%) were purchased from iTASCO.

### 3.2 Preparation of DDAF precursor

DDAB (231 mg, 0.5 mmol) and NaF (21 mg, 0.5 mmol) were dissolved in toluene (5 ml) and DI water (5 ml). Prepared solution was then reacted under sonication for 30 min for exchange of the bromide anions with fluoride anions. Then, the thick white mixture solution was centrifuged under 8000 rpm for 10 min and finally DDAF solution in toluene was obtained.

### 3.3 Synthesis of CsPbBr<sub>3</sub> nanocrystals

**Cs-oleate solution:** 407 mg of cesium carbonate, 1.25 ml of OAc, and 20 ml of ODE were added to a 3-necked round-bottom flask and stirred under vacuum for 60 min at 120 °C for degassing to remove impurities. Then the temperature was risen to 150 °C for 30 min under N<sub>2</sub> to completely make Cs-oleate solution in ODE.

**CsPbBr<sub>3</sub> NCs synthesis:** 398 mg of PbBr<sub>2</sub>, 2.5 ml of OLA, 2.5 ml of OAc and 25 mL of ODE were stirred in round-bottom flask and degassed under vacuum at 120 °C for 60 min. The flask was then filled with N<sub>2</sub>. The temperature of flask was risen to 150 °C for 30min under N<sub>2</sub> until the PbBr<sub>2</sub> completely dissolved. Subsequently, the temperature of PbBr<sub>2</sub> solution was then increased to 180 °C. When the temperature of the PbBr<sub>2</sub> solution reaches

180 °C, 2 ml of Cs-oleate was swiftly injected into the PbBr<sub>2</sub> solution. The reaction mixture was reacted at 180 °C for 10 seconds, immediately, a mixture solution was put into the ice bath to stop the reaction. When the temperature of mixture solution in round-bottom flask was cooled down into 60 °C, Then the light green colored CsPbBr<sub>3</sub> nanocrystal crude solution is prepared.

**Purification:** The crude solution was divided into 2 conical tubes of 50 ml volume ~ 15 ml each, and precipitated by addition of 35 ml of MeOAc (until the maximum capacity of conical tubes) and then centrifuged at 8000 rpm for 3 min. The precipitates of PNCs from centrifuge were redispersed in 5 ml of hexane, precipitated again with 7.5 ml of MeOAc, and centrifuged again at 8000 rpm for 3 min. The final precipitates of PNCs were redispersed only in 5 ml of hexane and centrifuged again at 8000 rpm for 3 min to remove untargeted size of PNCs.

### **3.4 Synthesis of Cadmium acetate treated CsPbBr<sub>3</sub> Nanocrystals**

In this procedure, 0.2 ml of DDAF solution was added to the CsPbBr<sub>3</sub>/toluene stock solution (8 mg/ml) with stirring for 30 min at room temperature.

For the CdAc treated CsPbBr<sub>3</sub> solution, ~ 0.012 mmol of cadmium acetate was added into 10 ml of toluene and sonicated for 30 min to make the mixture widely dissolved. After that, the solution was kept at room temperature for 1 hour to get a finely MeOAc distributed solution. The CdAc treated CsPbBr<sub>3</sub> is made by adding MeOAc distributed solution into same concentration of upper CsPbBr<sub>3</sub>/toluene stock solution. After reaction, mixture was centrifuged with MeOAc (reaction mixture: MeOAc is 1:3) at 9000 rpm for 3 min. The precipitates were redispersed in 1 ml of hexane for centrifugation again and then the supernatant was collected as the CdAc treated CsPbBr<sub>3</sub> PNCs solution.

### **3.5 Device fabrication and characterization**

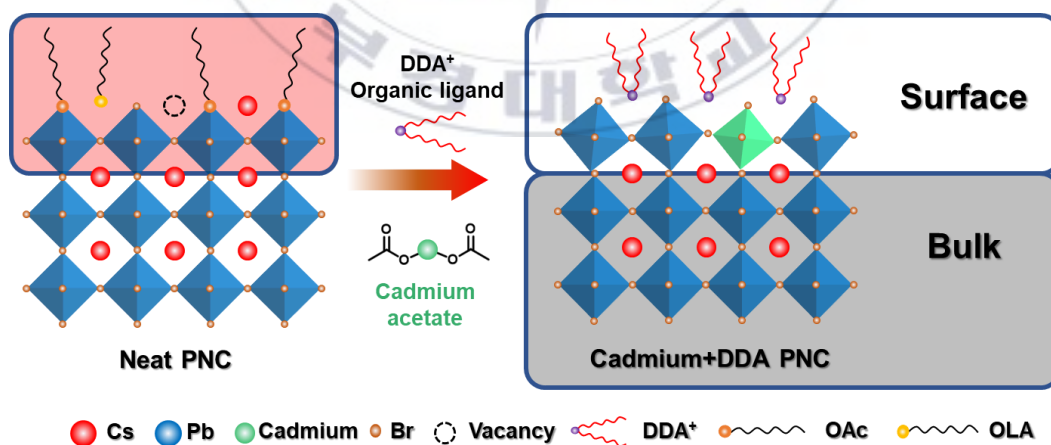
For perovskite LED devices, the glass / ITO substrates were exposed to oxygen plasma for 15 min to make the surface hydrophilic. PEDOT:PSS solution was spin coated at 4500 rpm for 40 sec and subsequently annealed at 150 °C for 20 min in the ambient air. After that, TFB (10 mg/ml) and PTAA (12 mg/ml) were spin coated at 4000 rpm for 40 sec as following HTL and annealed at 100 °C for 20 min in the nitrogen atmosphere individually. CsPbBr<sub>3</sub> PNCs (dispersed in octane, 5 mg/ml) were spin coated at 2000 rpm for 40 seconds. The ETL was evaporated in  $1 \times 10^{-6}$  torr vacuum

pressure using a thermal evaporator with thickness of TPBi (~ 70 nm), LiF (~ 2 nm), and Al (~ 100 nm) each. In this procedure, only TPBi was deposited on the whole side.

## Chapter 4. Result and Discussion

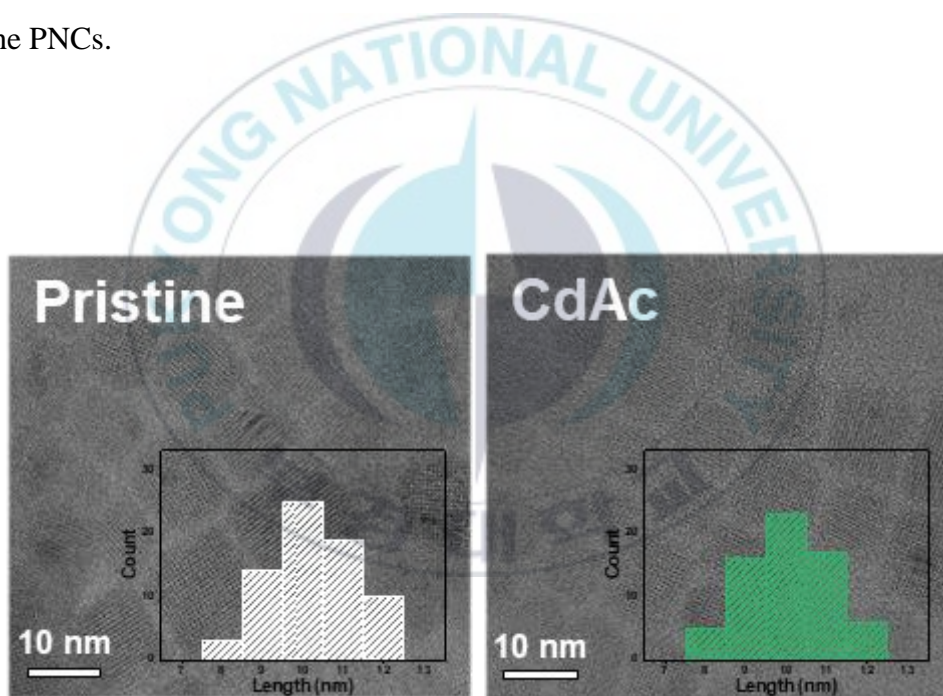
### 4.1 Concept of Surface passivation and TEM & PXRD analysis

Figure 4 shows a diagrammatic representation of the CdAc treatment process utilized for the ligand exchange process in the PNCs solution. Our study introduces a novel approach for filling the lead (Pb) vacancy on the surface of PNCs by incorporating CdAc during the ligand exchange process.



**Figure 4.** Schematic illustration of PNCs defect passivation and ligand exchange process

The use of organic-inorganic surface engineering maintained the original size and cube shape of the PNCs ( $\sim 10$  nm) in comparison to the as-synthesized PNCs, as shown in Figure 5 through TEM analysis. The TEM images of each PNCs revealed uniform cubic shape, with edge lengths of  $10.30 \pm 0.99$  and  $10.02 \pm 1.10$  nm respectively. Low magnification TEM images of CdAc-treated PNCs were shown in Figure 6, and EDS mapping images of Cs, Pb, Cd and Br atoms overlapped well with the TEM images, indicating the presence of each component in the PNCs.



**Figure 5.** High magnification TEM image of pristine and CdAc treated  $\text{CsPbBr}_3$  nanocrystals, size histogram of PNCs (inset)

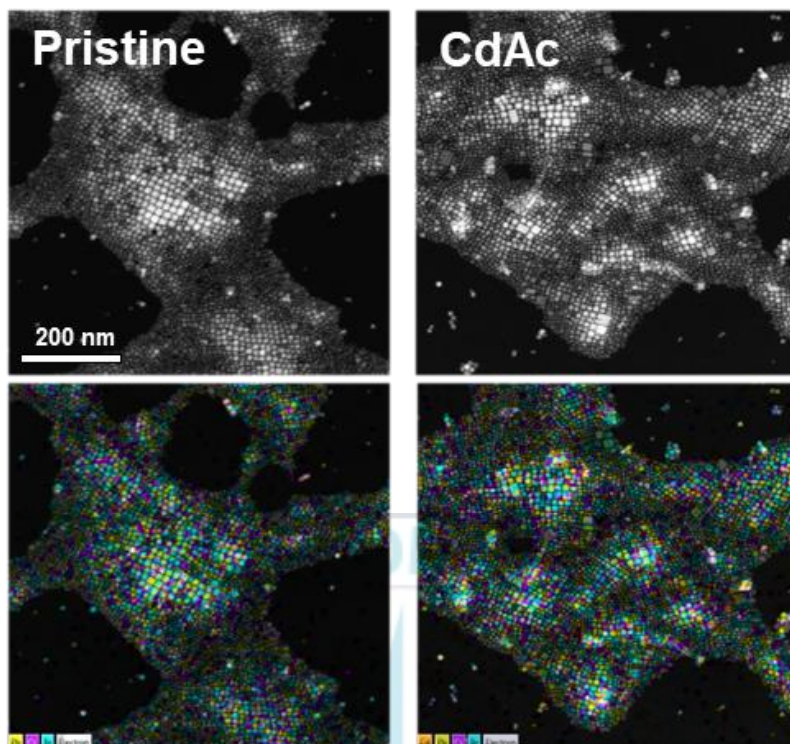


**Figure 6.** Low magnification TEM image of pristine and CdAc treated CsPbBr<sub>3</sub> PNCs and EDS mapping images of Cs, Pb, Cd and Br atoms

Following the treatment of PNCs with CdAc, the level of crystallinity was examined through the application of powder X-ray diffraction (PXRD) analysis in Figure 7. Results from the PXRD pattern indicated that the cadmium ions remained on the surface of the PNCs rather than integrating into the perovskite lattice, as there was no shift in the reflection angle. If the metal ions were smaller than Pb<sup>2+</sup> ion, peak shifts to higher diffraction angles may have occurred.<sup>[61]</sup> The outcomes, however, demonstrate that the perovskite's structural integrity remains unaltered

following the treatment with cadmium ions and that only surface defects are affected.

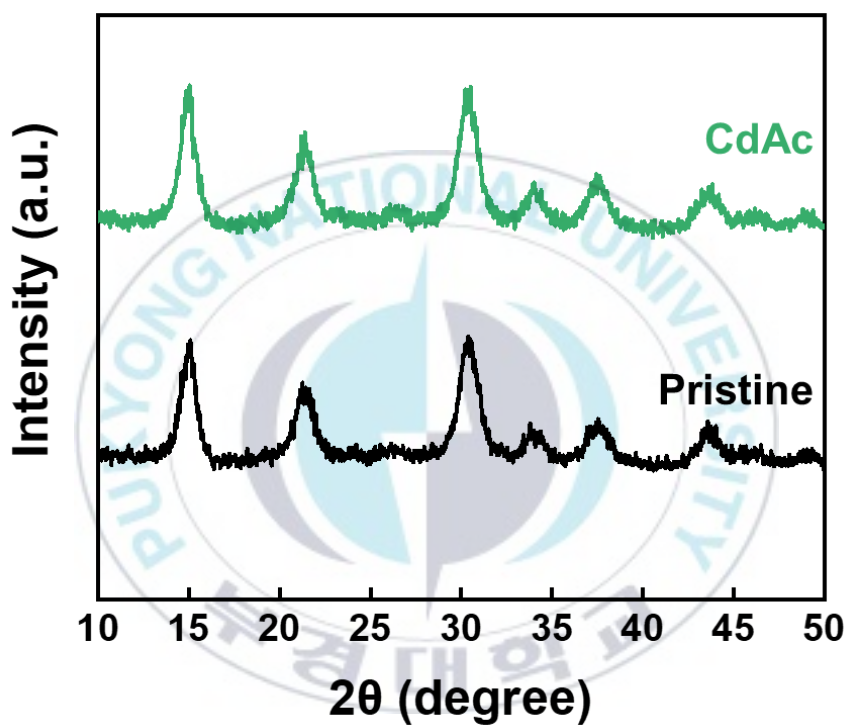


**Figure 7.** Powder X-ray diffraction pattern for pristine and CdAc treated PNCs

## 4.2 Fourier-transform infrared spectroscopy and Optical analysis

The effectiveness of replacing the original ligands (OAc, OLA) with DDA<sup>+</sup> on the PNCs was verified using Fourier-transform infrared (FT-IR) spectroscopy (Figure 8).

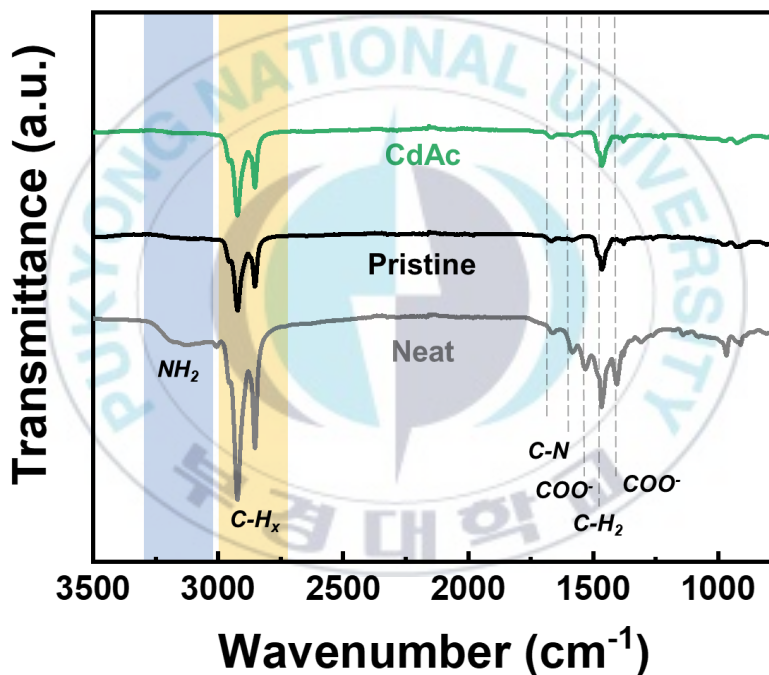


**Figure 8.** Fourier-transform infrared spectroscopy of neat, pristine and CdAc treated PNCs

All green-emitting PNCs have the identical UV-visible absorption and PL spectra at 514 nm, as observed in Figure 9. No new dopant emission or shifts in the

emission peaks were observed. These findings indirectly suggest that the surface passivation process was successful in treating the CdAc, without bulk doping.

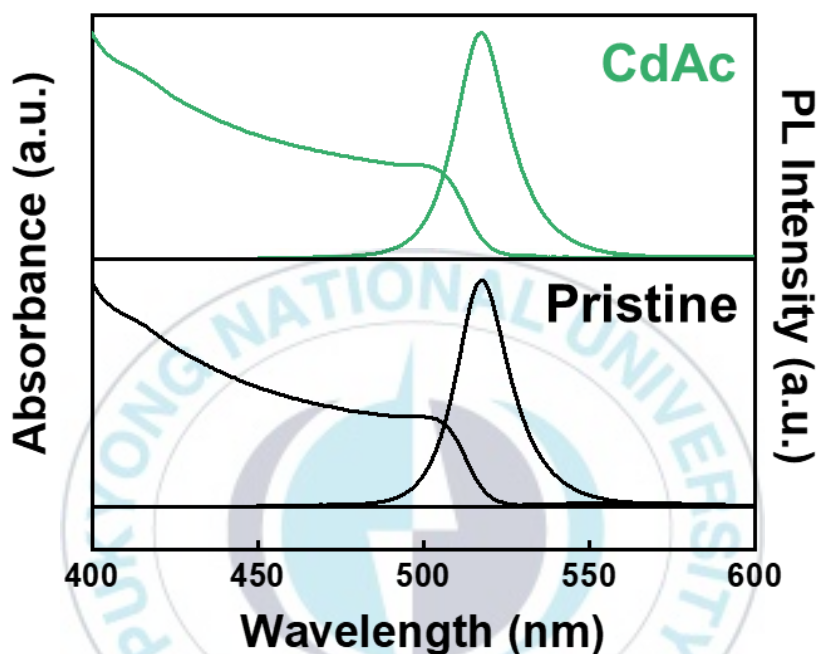


**Figure 9.** Normalized absorption and PL spectra and UV-visible absorption of the pristine and CdAc treated PNCs

To explore whether surface defects of the PNCs were being passivated by treating them with additional CdAc, time-resolved photoluminescence (TRPL) decay and PLQY measurements were conducted. The decay curves of PL were analyzed using a multi-exponential function (Figure 10). The average lifetime of PL ( $\tau_{\text{avg}}$ ) of the PNCs solutions increased from 9.04 (for pristine samples) to 10.80 (for CdAc-treated samples).

And the PLQY of the PNCs solution was measured for both pristine and CdAc treated solutions, resulting in 67.18% (pristine) and 96.02% (CdAc) respectively. (Figure 11)

This indicates that the optical properties of the PNCs are enhanced by the additional CdAc treatment, and this trend is consistent with the TRPL data. The results suggest that the CdAc treatment can reduce the density of surface traps, leading to stronger radiative recombination and lower PL quenching of PNCs. Thus, it demonstrates that this treatment can effectively control the trapped carriers on the surface, making PNCs suitable for stable and highly efficient optoelectronic devices.

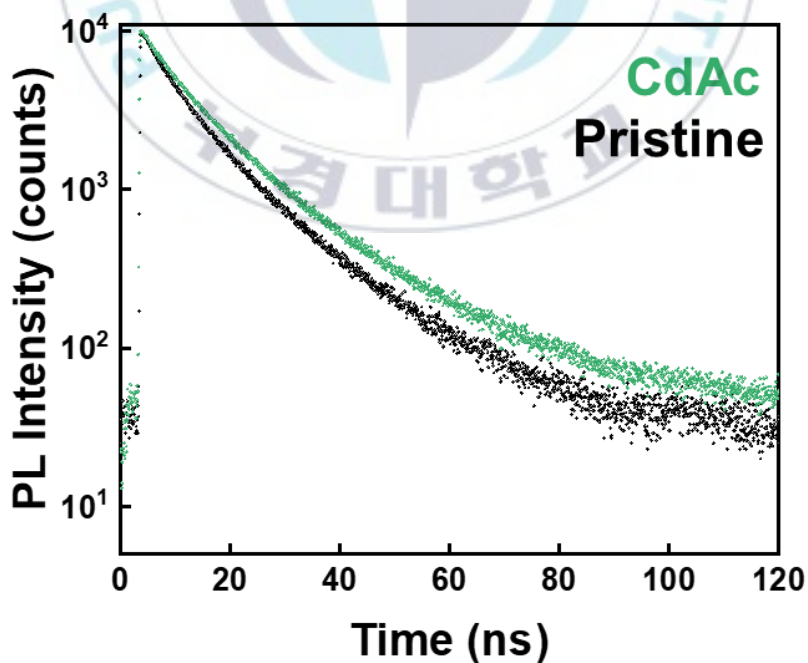


**Figure 10.** PL decay curves of the pristine and CdAc treated PNCs

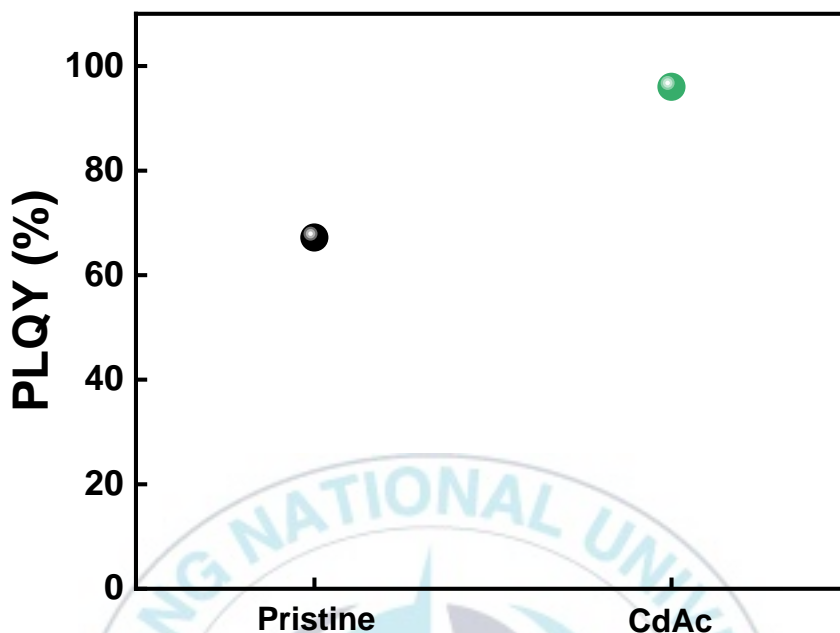


**Figure 11.** Solution PLQY plots of the pristine and CdAc treated PNCs

In addition, I analyzed the stability of PNCs films with pristine and CdAc treatment. I deposited all PNCs films on a glass substrate and put them under ambient conditions (20 °C, 40% relative humidity). Figure 11 shows the PLQY results of each PNCs film over time and images of the PL under UV lamp illumination are shown in Figure 12. Within 7 days, the pristine film exhibited swift degradation caused by surface defects, whereas CdAc treated films maintained a stable emission even after 14 days (~50% of the initial intensity). (Figure 13)

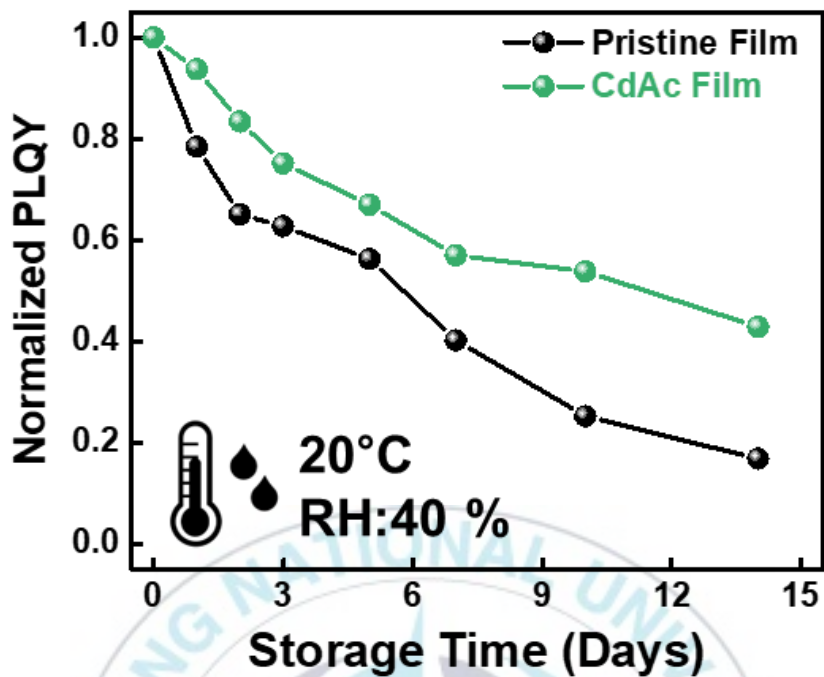


**Figure 12.** Time dependent storage film PLQY plots of the pristine and CdAc treated PNCs

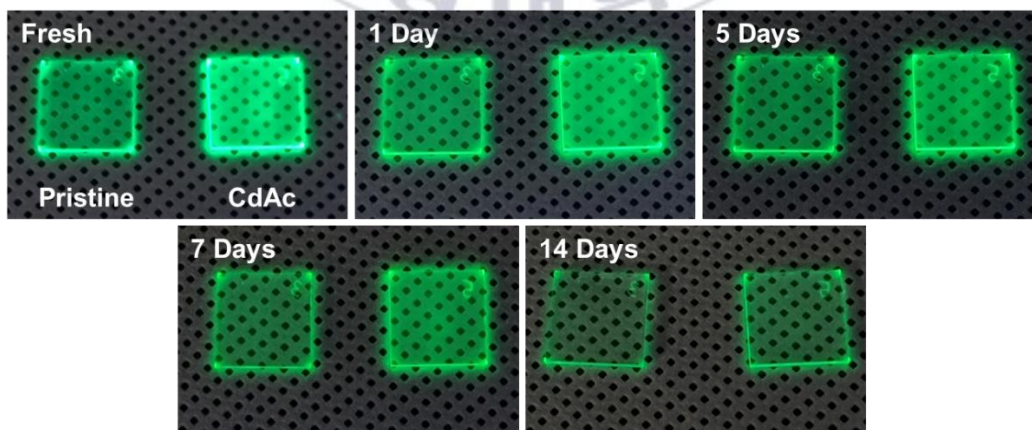


**Figure 13.** Photo of Time dependent storage film of the pristine and CdAc treated PNCs

### 4.3 Electrical analysis on PNCs and Perovskite LED

To investigate how CdAc treatment affects the defect density of PNCs, it has been conducted fabrication of hole-only devices (ITO / HTLs / PNCs / MoO<sub>3</sub> / Ag) and obtained the trap-filled limit voltage ( $V_{TFL}$ ) from the  $J$ - $V$  curve of the devices (Figure 14). A lower  $V_{TFL}$  value indicates a lower trap density in the PNCs.<sup>[62]</sup>  $V_{TFL}$  was reduced from 0.52 V (pristine) to 0.34 V (CdAc). The trap state density of PNCs can be calculated using the following equation.<sup>[63]</sup>

$$N_t = \frac{2\epsilon\epsilon_0 V_{TFL}}{eL^2}$$

Eq.4.1

The dielectric constant of CsPbBr<sub>3</sub> (~ 16.46) and vacuum permittivity (8.854 × 10<sup>-12</sup> F m<sup>-1</sup>) are represented as  $\epsilon$  and  $\epsilon_0$ , respectively. The elementary charge (1.6 × 10<sup>-19</sup> Coulombs) is denoted as  $e$ , and the thickness of the PNCs film is represented as  $L$  (~ 40 nm). The trap densities ( $N_t$ ) of pristine and CdAc treated PNCs were calculated to be 1.78 × 10<sup>17</sup> cm<sup>-3</sup> and 1.17 × 10<sup>17</sup> cm<sup>-3</sup>, respectively. This indicates that the CdAc treatment process effectively controls the surface defect and reduces the defect density. These results demonstrate that exciton quenching and trap formation in the perovskite film are significantly minimized by the CdAc treatment process.

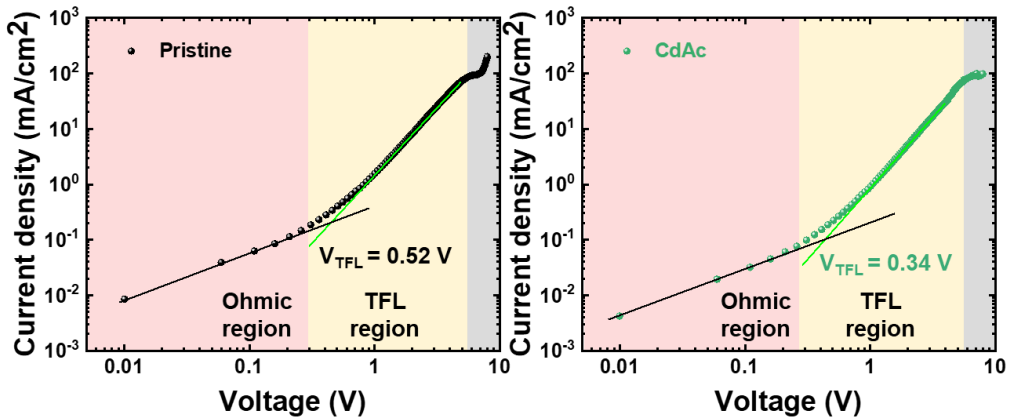


**Figure 14.**  $J$ - $V$  characteristics of hole-only devices with  $V_{TFL}$  kink point behavior in pristine and CdAc treated PNCs films.

To verify the effectiveness of PNCs in optoelectronic devices, I created perovskite LEDs utilizing both the pristine and CdAc treated PNCs. The energy level diagram of the perovskite LED used in our study can be found in Figure 15, and the results of the ultraviolet photoelectron spectroscopy (UPS) can be seen in Figure 16. Figure 17 a-d show the device performances; a) Current density *versus* voltage, b) Luminance *versus* voltage, c) Current density *versus* EQE and d) EL spectra at  $EQE_{max}$  of perovskite LED respectively. Through a comparison of the performance of perovskite LEDs fabricated with pristine and CdAc treated PNCs, the positive impact of CdAc treatment on PNCs is evident. The maximum luminance and  $EQE_{max}$  of the pristine perovskite LED were  $684 \text{ cd m}^{-2}$  and 14.32%, respectively. Conversely, the perovskite LED using CdAc treatment on PNCs

showed a significant improvement, with maximum luminance and  $EQE_{\max}$  values of  $1175 \text{ cd m}^{-2}$  and 20.79%, respectively. The EL spectra of both devices appeared at 514 nm with 20 nm full width at half maximum (FWHM), which is the same as the PL spectrum. Moreover, the EL spectrum of the perovskite LED using CdAc treatment on PNCs remained stable at 514 nm for voltages ranging from 2.7 V to 4.5 V (Figure 18). More detailed performance parameters of each perovskite LED device can be found in Table 1.

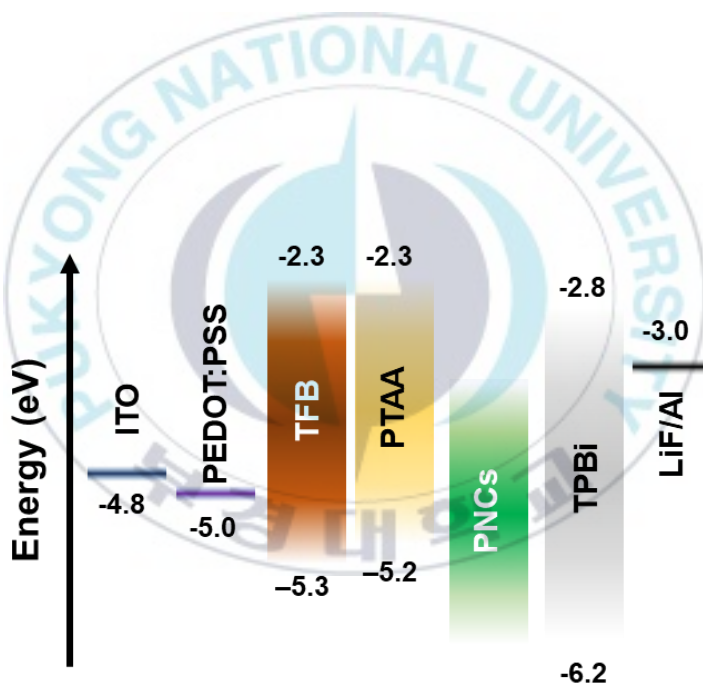


**Figure 15.** Energy level diagram of perovskite LED device

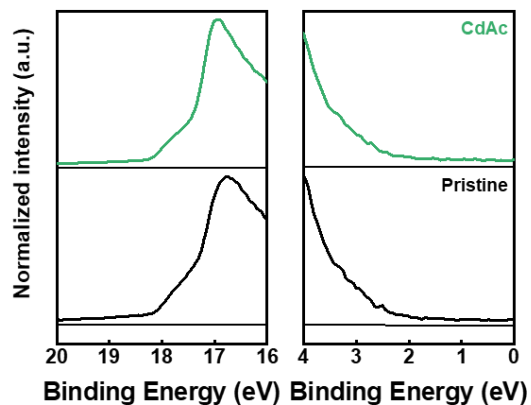


**Figure 16.** UPS spectra of pristine and CdAc treated PNCs

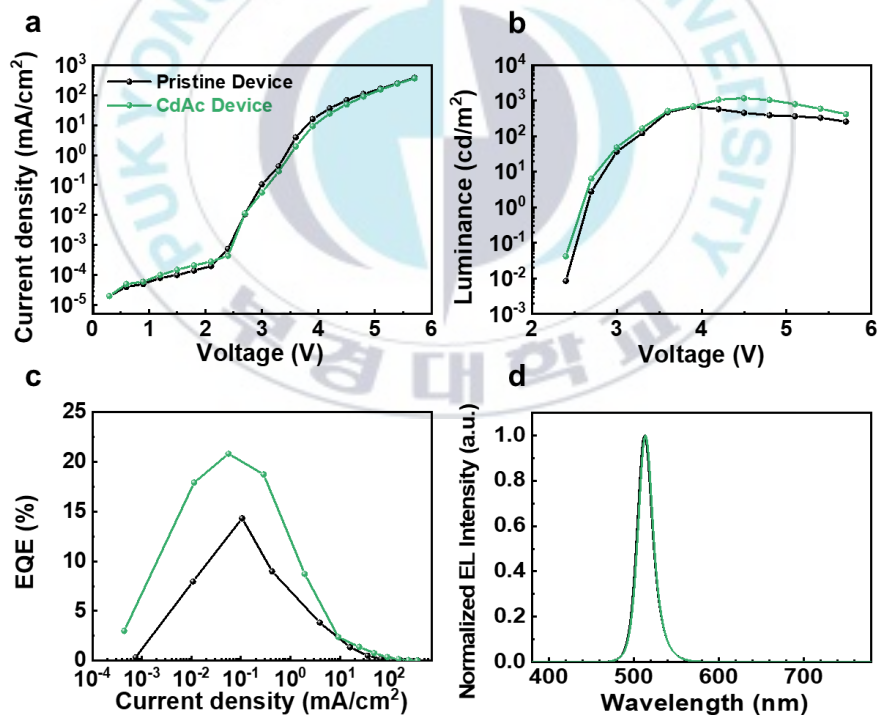


**Figure 17.** a) Current density–voltage ( $J$ – $V$ ) curves of perovskite LED device. b) Luminance–voltage ( $L$ – $V$ ) curves of perovskite LED device. c) Current density–EQE curves of perovskite LED device. d) EL spectra at  $\text{EQE}_{\text{max}}$  of perovskite LED

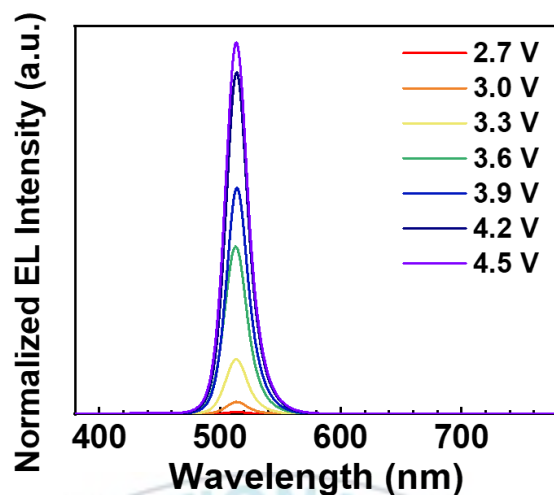


Figure 18. EL spectra with voltage from 2.7 V to 4.5 V

Sample configuration	$L_{\max}$ [cd/m <sup>2</sup> ] @ bias	$LE_{\max}$ [cd/A] @ bias	$EQE_{\max}$ [%] @ bias	Turn-on Voltage[V] @ 1cd/m <sup>2</sup>	Wavelength [nm]
Pristine	530@3.6	47.68@3.0	14.72@3.0	2.7	514
CdAc	1175@4.5	65.48@3.0	20.79@3.0	2.7	514

Table 1. Summarized device performances with pristine and CdAc treated device

The stability of each PNCs in ambient conditions was confirmed through PL stability analysis (Figure 12, 13). Subsequently, operational stability measurement ( $T_{50}$ ) and joule heat control were performed to investigate the stability of the pristine and CdAc treated devices based on the stability of PNCs (Figure 19, 21). Figure 19 shows the operational stability of perovskite LEDs fabricated with

pristine and CdAc treated PNCs under constant current densities of 0.03, ~0.60, and ~1.7 mA cm<sup>-2</sup>. Although CdAc treated perovskite LEDs have similar current densities with pristine perovskite LEDs, they exhibit higher initial luminance values. Moreover, the decay time to 50% ( $T_{50}$ ) from the initial luminance in CdAc treated device is 1.1, 2.1, and 8.7 min, respectively, which is approximately 1.3 times longer than that of the pristine device (6.7 min). Additionally, both devices demonstrate stable green emission of similar spectra at each point of  $T_{100}$ ,  $T_{75}$ , and  $T_{50}$  as shown in Figure 20. During the operation of the devices, their temperatures were recorded using an infrared thermal imaging camera, as depicted in Figure 21. The temperature of both pristine and CdAc treated devices was measured at 33 mA cm<sup>-2</sup>, and the values were found to be 26.53 °C and 24.34 °C, respectively, at the maximum luminance voltage of 4.5 V. Thus, the outcomes of this thesis suggest that the CdAc treatment process helps to fill the surface defects present on the PNCs surface and reduce lattice strain, which in turn may lead to the suppression of thermal-induced joule heating of perovskite LEDs through surface CdAc treatment.<sup>[64]</sup>

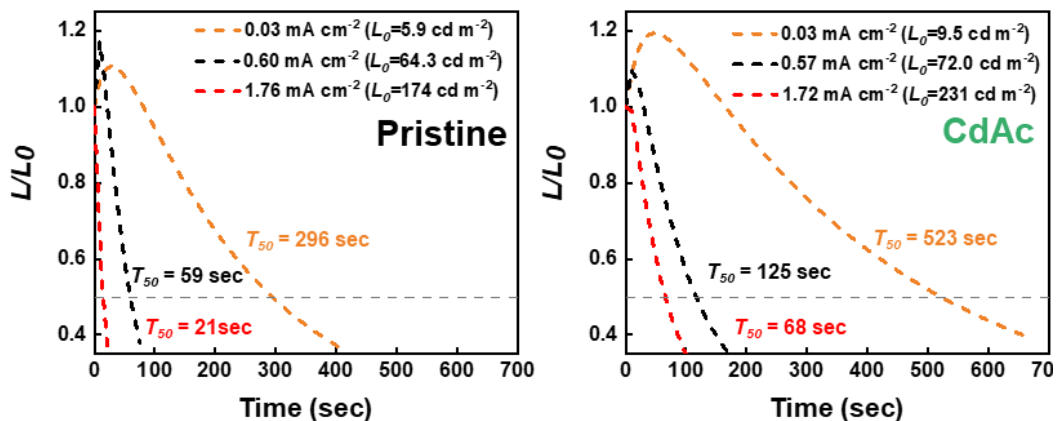


Figure 19. Operational stability of pristine and CdAc treated perovskite LEDs measured at each current densities

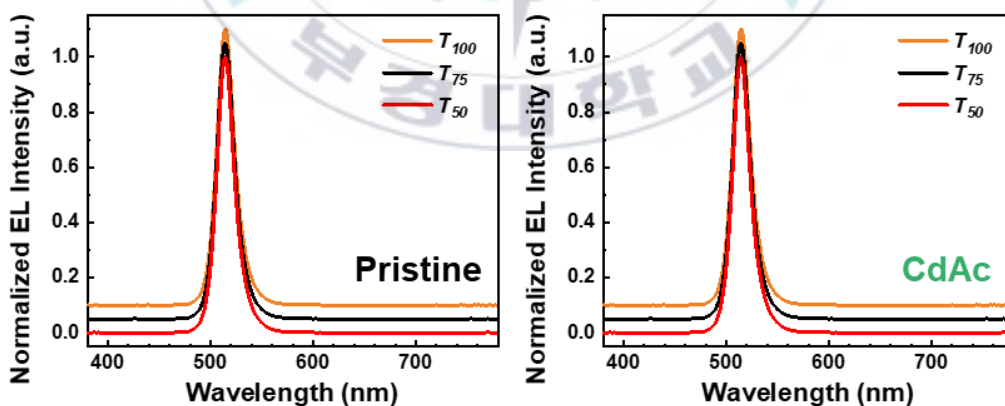
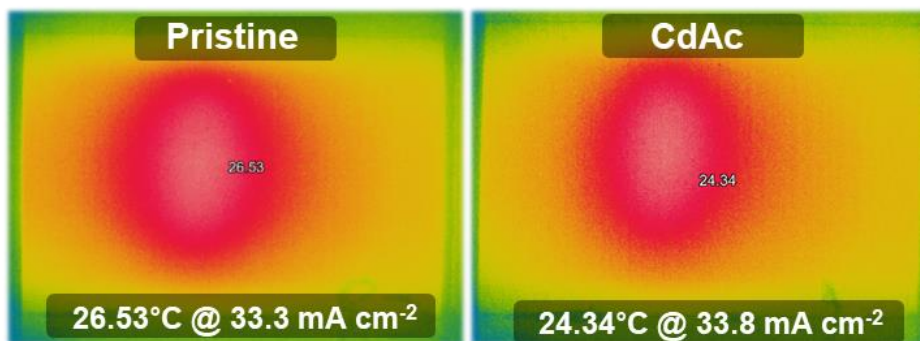


Figure 20. EL spectra at each point of operation



**Figure 21.** The temperature of both devices measured with an IR thermal imaging camera during the device's operation

## Chapter 5. Conclusion

In summary, I successfully demonstrate simple and effective CdAc post treatment strategy with organic ligand on perovskite LED. The use of CdAc has demonstrated to be effective in reducing surface defects in PNCs, resulting in superior optical and electrical characteristics compared to pristine PNCs. Moreover, the excellent characteristics of these PNCs were evident from the TRPL analysis, which did not show any dopant emission or alterations in the crystal structure. Furthermore, the CdAc treatment led to PNCs with low trap density and high PLQY, resulting in highly efficient perovskite LEDs. These characteristics also played a crucial role in the stability of both the materials and devices, and thus, PNCs and perovskite LEDs treated with CdAc exhibited outstanding PL and EL stability.

## Reference

- [1] M.-H. Jung, S. H. Rhim, D. Moon, *Solar Energy Materials and Solar Cells* **2017**, 172, 44.
- [2] D. B. Mitzi, *Journal of the Chemical Society, Dalton Transactions* **2001**, 10, 1039
- [3] L. Liang, L. Wencong, C. Nianyi, *Journal of Physics and Chemistry of Solids* **2004**, 65, 855.
- [4] F. Deschler, M. Price, S. Pathak, L. E. Klintberg, D.-D. Jarausch, R. Higler, S. Hüttner, T. Leijtens, S. D. Stranks, H. J. Snaith, M. Atatüre, R. T. Phillips, R. H. Friend, *The Journal of Physical Chemistry Letters* **2014**, 5, 1421.
- [5] Z.-K. Tan, R. S. Moghaddam, M. L. Lai, P. Docampo, R. Higler, F. Deschler, M. Price, A. Sadhanala, L. M. Pazos, D. Credgington, F. Hanusch, T. Bein, H. J. Snaith, R. H. Friend, *Nature Nanotechnology* **2014**, 9, 687.
- [6] V. D’Innocenzo, A. R. Srimath Kandada, M. De Bastiani, M. Gandini, A. Petrozza, *Journal of the American Chemical Society* **2014**, 136, 17730.
- [7] S. D. Stranks, H. J. Snaith, *Nature Nanotechnology* **2015**, 10, 391.
- [8] W.-J. Yin, T. Shi, Y. Yan, *Applied Physics Letters* **2014**, 104, 063903.
- [9] D. W. de Quilettes, S. M. Vorpahl, S. D. Stranks, H. Nagaoka, G. E. Eperon, M. E. Ziffer, H. J. Snaith, D. S. Ginger, *Science* **2015**, 348, 683.
- [10] L. C. Schmidt, A. Pertegás, S. González-Carrero, O. Malinkiewicz, S. Agouram, G. Mínguez Espallargas, H. J. Bolink, R. E. Galian, J. Pérez-Prieto, *Journal of the American Chemical Society* **2014**, 136, 850.
- [11] D. Zhang, Y. Yu, Y. Bekenstein, A. B. Wong, A. P. Alivisatos, P. Yang, *Journal of the American Chemical Society* **2016**, 138, 13155.
- [12] J. A. Sichert, Y. Tong, N. Mutz, M. Vollmer, S. Fischer, K. Z. Milowska, R. García Cortadella, B. Nickel, C. Cardenas-Daw, J. K. Stolarczyk, A. S. Urban, J. Feldmann, *Nano Letters* **2015**, 15, 6521.
- [13] A. B. Wong, Y. Bekenstein, J. Kang, C. S. Kley, D. Kim, N. A. Gibson, D. Zhang, Y. Yu, S. R. Leone, L.-W. Wang, A. P. Alivisatos, P. Yang, *Nano Letters* **2018**, 18, 2060.
- [14] Q. A. Akkerman, S. G. Motti, A. R. Srimath Kandada, E. Mosconi, V. D’Innocenzo, G. Bertoni, S. Marras, B. A. Kamino, L. Miranda, F. De Angelis, A. Petrozza, M. Prato, L. Manna, *Journal of the American Chemical Society* **2016**, 138, 1010.
- [15] Q. A. Akkerman, V. D’Innocenzo, S. Accornero, A. Scarpellini, A. Petrozza, M. Prato, L. Manna, *Journal of the American Chemical Society* **2015**, 137, 10276.
- [16] G. Nedelcu, L. Protesescu, S. Yakunin, M. I. Bodnarchuk, M. J. Grotevent, M. V. Kovalenko, *Nano Letters* **2015**, 15, 5635.
- [17] V. A. Hintermayr, A. F. Richter, F. Ehrat, M. Döblinger, W. Vanderlinden, J. A. Sichert, Y. Tong, L. Polavarapu, J. Feldmann, A. S. Urban, *Advanced Materials* **2016**, 28, 9478.
- [18] Y. Tong, F. Ehrat, W. Vanderlinden, C. Cardenas-Daw, J. K. Stolarczyk, L. Polavarapu, A. S. Urban, *ACS Nano* **2016**, 10, 10936.

- [19] S. Gonzalez-Carrero, L. Francés-Soriano, M. González-Béjar, S. Agouram, R. E. Galian, J. Pérez-Prieto, *Small* **2016**, 12, 5245.
- [20] F. Di Stasio, S. Christodoulou, N. Huo, G. Konstantatos, *Chemistry of Materials* **2017**, 29, 7663.
- [21] C. M. M. Soe, G. P. Nagabhushana, R. Shivaramaiah, H. Tsai, W. Nie, J.-C. Blancon, F. Melkonyan, D. H. Cao, B. Traoré, L. Pedesseau, M. Kepenekian, C. Katan, J. Even, T. J. Marks, A. Navrotsky, A. D. Mohite, C. C. Stoumpos, M. G. Kanatzidis, *Proceedings of the National Academy of Sciences* **2019**, 116, 58.
- [22] B. J. Bohn, Y. Tong, M. Gramlich, M. L. Lai, M. Döblinger, K. Wang, R. L. Z. Hoyer, P. Müller-Buschbaum, S. D. Stranks, A. S. Urban, L. Polavarapu, J. Feldmann, *Nano Letters* **2018**, 18, 5231.
- [23] Y. Zheng, T. Niu, X. Ran, J. Qiu, B. Li, Y. Xia, Y. Chen, W. Huang, *Journal of Materials Chemistry A* **2019**, 7, 13860.
- [24] F. Wang, S. Bai, W. Tress, A. Hagfeldt, F. Gao, *npj Flexible Electronics* **2018**, 2, 22.
- [25] H. Uratani, K. Yamashita, *The Journal of Physical Chemistry Letters* **2017**, 8, 742.
- [26] S. Gonzalez-Carrero, R. E. Galian, J. Pérez-Prieto, *Journal of Materials Chemistry A* **2015**, 3, 9187.
- [27] L. Protesescu, S. Yakunin, M. I. Bodnarchuk, F. Krieg, R. Caputo, C. H. Hendon, R. X. Yang, A. Walsh, M. V. Kovalenko, *Nano Letters* **2015**, 15, 3692.
- [28] F. Zhang, H. Zhong, C. Chen, X.-g. Wu, X. Hu, H. Huang, J. Han, B. Zou, Y. Dong, *ACS Nano* **2015**, 9, 4533.
- [29] J. De Roo, M. Ibáñez, P. Geiregat, G. Nedelcu, W. Walravens, J. Maes, J. C. Martins, I. Van Driessche, M. V. Kovalenko, Z. Hens, *ACS Nano* **2016**, 10, 2071.
- [30] R. K. Behera, S. Das Adhikari, S. K. Dutta, A. Dutta, N. Pradhan, *The Journal of Physical Chemistry Letters* **2018**, 9, 6884.
- [31] B. A. Koscher, J. K. Swabeck, N. D. Bronstein, A. P. Alivisatos, *Journal of the American Chemical Society* **2017**, 139, 6566.
- [32] S. Chang, Z. Bai, H. Zhong, *Advanced Optical Materials* **2018**, 6, 1800380.
- [33] Y. Wei, Z. Cheng, J. Lin, *Chemical Society Reviews* **2019**, 48, 310.
- [34] L. N. Quan, F. P. García de Arquer, R. P. Sabatini, E. H. Sargent, *Advanced Materials* **2018**, 30, 1801996.
- [35] B. Zhao, S. Bai, V. Kim, R. Lamboll, R. Shivanna, F. Auras, J. M. Richter, L. Yang, L. Dai, M. Alsari, X.-J. She, L. Liang, J. Zhang, S. Lilliu, P. Gao, H. J. Snaith, J. Wang, N. C. Greenham, R. H. Friend, D. Di, *Nature Photonics* **2018**, 12, 783.
- [36] K. Lin, J. Xing, L. N. Quan, F. P. G. de Arquer, X. Gong, J. Lu, L. Xie, W. Zhao, D. Zhang, C. Yan, W. Li, X. Liu, Y. Lu, J. Kirman, E. H. Sargent, Q. Xiong, Z. Wei, *Nature* **2018**, 562, 245.
- [37] X. Jiang, F. Wang, Q. Wei, H. Li, Y. Shang, W. Zhou, C. Wang, P. Cheng, Q. Chen, L. Chen, Z. Ning, *Nature Communications* **2020**, 11, 1245.
- [38] W. Xiang, W. Tress, *Advanced Materials* **2019**, 31, 1902851.
- [39] W. Pan, H. Wu, J. Luo, Z. Deng, C. Ge, C. Chen, X. Jiang, W.-J. Yin, G. Niu, L. Zhu, L. Yin, Y. Zhou, Q. Xie, X. Ke, M. Sui, J. Tang, *Nature Photonics* **2017**, 11, 726.

- [40] X.-K. Liu, W. Xu, S. Bai, Y. Jin, J. Wang, R. H. Friend, F. Gao, *Nature Materials* **2021**, 20, 10.
- [41] M.-H. Park, J. Park, J. Lee, H. S. So, H. Kim, S.-H. Jeong, T.-H. Han, C. Wolf, H. Lee, S. Yoo, T.-W. Lee, *Advanced Functional Materials* **2019**, 29, 1902017.
- [42] W. Xu, Q. Hu, S. Bai, C. Bao, Y. Miao, Z. Yuan, T. Borzda, A. J. Barker, E. Tyukalova, Z. Hu, M. Kawecki, H. Wang, Z. Yan, X. Liu, X. Shi, K. Uvdal, M. Fahlman, W. Zhang, M. Duchamp, J.-M. Liu, A. Petrozza, J. Wang, L.-M. Liu, W. Huang, F. Gao, *Nature Photonics* **2019**, 13, 418.
- [43] C. Cho, B. Zhao, G. D. Tainter, J.-Y. Lee, R. H. Friend, D. Di, F. Deschler, N. C. Greenham, *Nature Communications* **2020**, 11, 611.
- [44] T. Chiba, Y. Hayashi, H. Ebe, K. Hoshi, J. Sato, S. Sato, Y.-J. Pu, S. Ohisa, J. Kido, *Nature Photonics* **2018**, 12, 681.
- [45] L. Gao, L. N. Quan, F. P. García de Arquer, Y. Zhao, R. Munir, A. Proppe, R. Quintero-Bermudez, C. Zou, Z. Yang, M. I. Saidaminov, O. Voznyy, S. Kinge, Z. Lu, S. O. Kelley, A. Amassian, J. Tang, E. H. Sargent, *Nature Photonics* **2020**, 14, 227.
- [46] Z. Chu, Q. Ye, Y. Zhao, F. Ma, Z. Yin, X. Zhang, J. You, *Advanced Materials* **2021**, 33, 2007169.
- [47] C. Sun, Y. Jiang, M. Cui, L. Qiao, J. Wei, Y. Huang, L. Zhang, T. He, S. Li, H.-Y. Hsu, C. Qin, R. Long, M. Yuan, *Nature Communications* **2021**, 12, 2207.
- [48] Y. He, J. Yan, L. Xu, B. Zhang, Q. Cheng, Y. Cao, J. Zhang, C. Tao, Y. Wei, K. Wen, Z. Kuang, G. M. Chow, Z. Shen, Q. Peng, W. Huang, J. Wang, *Advanced Materials* **2021**, 33, 2006302.
- [49] Z. Li, Z. Chen, Y. Yang, Q. Xue, H.-L. Yip, Y. Cao, *Nature Communications* **2019**, 10, 1027.
- [50] X. Yang, X. Zhang, J. Deng, Z. Chu, Q. Jiang, J. Meng, P. Wang, L. Zhang, Z. Yin, J. You, *Nature Communications* **2018**, 9, 570.
- [51] Y. Dong, Y.-K. Wang, F. Yuan, A. Johnston, Y. Liu, D. Ma, M.-J. Choi, B. Chen, M. Chekini, S.-W. Baek, L. K. Sagar, J. Fan, Y. Hou, M. Wu, S. Lee, B. Sun, S. Hoogland, R. Quintero-Bermudez, H. Ebe, P. Todorovic, F. Dinic, P. Li, H. T. Kung, M. I. Saidaminov, E. Kumacheva, E. Spiecker, L.-S. Liao, O. Voznyy, Z.-H. Lu, E. H. Sargent, *Nature Nanotechnology* **2020**, 15, 668.
- [52] N. Wang, L. Cheng, R. Ge, S. Zhang, Y. Miao, W. Zou, C. Yi, Y. Sun, Y. Cao, R. Yang, Y. Wei, Q. Guo, Y. Ke, M. Yu, Y. Jin, Y. Liu, Q. Ding, D. Di, L. Yang, G. Xing, H. Tian, C. Jin, F. Gao, R. H. Friend, J. Wang, W. Huang, *Nature Photonics* **2016**, 10, 699.
- [53] H. Cho, S.-H. Jeong, M.-H. Park, Y.-H. Kim, C. Wolf, C.-L. Lee, J. H. Heo, A. Sadhanala, N. Myoung, S. Yoo, S. H. Im, R. H. Friend, T.-W. Lee, *Science* **2015**, 350, 1222.
- [54] J. S. Kim, J.-M. Heo, G.-S. Park, S.-J. Woo, C. Cho, H. J. Yun, D.-H. Kim, J. Park, S.-C. Lee, S.-H. Park, E. Yoon, N. C. Greenham, T.-W. Lee, *Nature* **2022**, 611, 688.
- [55] A. Dutta, R. K. Behera, P. Pal, S. Baitalik, N. Pradhan, *Angewandte Chemie International Edition* **2019**, 58, 5552.

- [56] M. Imran, J. Ramade, F. Di Stasio, M. De Franco, J. Buha, S. Van Aert, L. Goldoni, S. Lauciello, M. Prato, I. Infante, S. Bals, L. Manna, *Chemistry of Materials* **2020**, 32, 10641.
- [57] L. M. Wheeler, E. M. Sanehira, A. R. Marshall, P. Schulz, M. Suri, N. C. Anderson, J. A. Christians, D. Nordlund, D. Sokaras, T. Kroll, S. P. Harvey, J. J. Berry, L. Y. Lin, J. M. Luther, *Journal of the American Chemical Society* **2018**, 140, 10504.
- [58] H. Wu, J. Pi, D. Zhou, Q. Wang, Z. Long, J. Qiu, *Ceramics International* **2022**, 48, 3383.
- [59] W. H. Jeong, Z. Yu, L. Gregori, J. Yang, S. R. Ha, J. W. Jang, H. Song, J. H. Park, E. D. Jung, M. H. Song, S. H. Park, H. J. Snaith, A. Boretti, F. De Angelis, D. Meggiolaro, J. Lee, H. Choi, B. R. Lee, *Journal of Materials Chemistry A* **2021**, 9, 26750.
- [60] M. Liu, N. Jiang, H. Huang, J. Lin, F. Huang, Y. Zheng, D. Chen, *Chemical Engineering Journal* **2021**, 413, 127547.
- [61] Z. Yang, M. Wei, O. Voznyy, P. Todorovic, M. Liu, R. Quintero-Bermudez, P. Chen, J. Z. Fan, A. H. Proppe, L. N. Quan, G. Walters, H. Tan, J.-W. Chang, U. S. Jeng, S. O. Kelley, E. H. Sargent, *Journal of the American Chemical Society* **2019**, 141, 8296.
- [62] D. Luo, W. Yang, Z. Wang, A. Sadhanala, Q. Hu, R. Su, R. Shivanna, G. F. Trindade, J. F. Watts, Z. Xu, T. Liu, K. Chen, F. Ye, P. Wu, L. Zhao, J. Wu, Y. Tu, Y. Zhang, X. Yang, W. Zhang, R. H. Friend, Q. Gong, H. J. Snaith, R. Zhu, *Science* **2018**, 360, 1442.
- [63] M. I. Saidaminov, M. A. Haque, J. Almutlaq, S. Sarmah, X.-H. Miao, R. Begum, A. A. Zhumekenov, I. Dursun, N. Cho, B. Murali, O. F. Mohammed, T. Wu, O. M. Bakr, *Advanced Optical Materials* **2017**, 5, 1600704.
- [64] Y. Shen, J. Zhou, Y. Li, J.-X. Tang, *The Journal of Physical Chemistry Letters* **2022**, 13, 6806.

## Acknowledgement

어느 덧 학부 3학년 6월부터 시작한 ODPL 연구실 생활을 마무리 짓는 시간이 다가와 학위논문을 마무리하고 새로운 시작을 할 때가 다가왔습니다. 지난 시간을 되돌아보며 연구를 알기 전과 후에 스스로의 모습을 되돌아보았을 때 많은 부분에서 변화가 일어났음을 느낄 수 있었습니다. 이 시간에 이르기까지 많은 도움과 관심을 주신 고마운 분들께 감사의 인사를 드리고자 합니다.

우선, 저에게 연구의 즐거움을 알게 해 주시고 연구를 진행함에 있어 아낌없는 지원과 동시에 조언이 필요할 때에는 아버지와 같이 항상 함께 논의해 주신 저의 지도교수님 박성흠 교수님께 깊은 감사의 말씀을 드리고 싶습니다. 어느 것 하나 이루고자 하는 목표가 없었던 저에게 지금과 같이 움직일 수 있는 바람을 일으켜 주신 가르침은 앞으로도 계속해서 저의 마음에 남아 있을 것입니다. 또한 항상 제자와 같이 연구를 진행할 수 있는 환경을 만들어 주시고, 조언이 필요할 때면 좋은 말씀을 전해 주시며 많은 관심과 격려를 아끼지 않아 주셨던 이보람 교수님께 감사말씀을 드립니다. 그리고 바쁘신 와중에도 귀중한 시간을 내어 논문심사를 해 주시고, 많은 조언과 함께 이제 내딛을 다음 발걸음을 이끌어 주신 최효성 교수님께 감사드립니다.

멀리 계시지만 언제나 선배로서 조언을 아끼지 않으시고 어른으로서 저에게 항상 필요한 말씀을 해주시는 이지훈 박사님, 한참 후배인 저에게 인자한 미소를 잃지 않으셨던 신인수 박사님, 걱정이 많을 때면 언제나 저를 응원해주었던 Pesi 박사님, 언젠가 저도 선배의 자리에 다다랐을 때 본받고 싶은 모습을 보여주었던 양현석 박사님, 행정 업무를 담당하시지만 제가 지쳐 보일때면 좋은 충고를 해주셨던 근녕이 누나, 아이와 같은 동심을 잃지 않고 옆에서 밝은 미소를 잃지 않아 주셨던 김단비 박사님, 옆자리에서 매번 큰 웃음을 만들어 주시는 은혜누나, 누구보다 착한 마음을 가지고 계시는 호준이형, 막내로서 웃음을 잃지 않고 이야기를 잘 들어주었던 유미, 지금은 본국으로 떠났지만 형으로서 많은 도움을 주었던 Yuan 박사님, 연구적 지식을 아낌없이 전해주었던 Fuqiang, 바람을 쐬러 나갈 때면 제 고민을 잘 들어주었던 Du, 마음이 잘 맞아 친구로서 의지할 수 있었던 Liying 과 Wu. 이렇게 저를 이끌어주고 함께 생활하며 너무나 많은 도움을 주신 ODPL 연구실 모든 인원들에게 감사말씀을 드리고 싶습니다. 그리고 옆 연구실에서 지금까지 셀 수 없는 많은 도움과 조언을 해 주시고 힘이 들 때면 의지할 수 있는 버팀목이 되어주며 하나의 연구를 처음부터 끝까지 이끌어 주었던 우현이형, 장난칠 때면 아이와 같다 가도 고민이 있을 때면 이야기를 잘 들어주었던 지원이 누나, 같은 연구실 후배처럼 저를 잘 따라주고 많은 도움이 되었던 지훈이와 경은이, 동생이지만 연구적으로 많은 고민을 해결해 주었던 동현이, 실험을 하다 가도 막힐 때면 달려와 주었던 Kai 에게 감사의 마음을 전합니다. 그리고 학위과정동안 많은 의지가 되었고 좋은 추억을 함께 만들 수 있게 해주었던 동혁이, 용이, 지원이, 민우, 기득이, 효원이를 포함한 우리 동기들에게 감사드립니다.

마지막으로 석사 학위를 받을 때까지 저를 믿어주고 부족함 없이 항상 지원을 아끼지 않으신 저의 가족에게 큰 감사의 마음을 전해드리고 싶습니다. 앞으로 더욱 스스로를 발전시키며 한층 더 성장한 연구자가 될 수 있도록 노력하여 좋은 모습을 보여드리겠습니다. 사랑하고 감사드립니다.